High Temp. Mater. Proc., Vol. **30** (2011), pp. 539–548 DOI 10.1515/HTMP.2011.111

Microstructure, Texture and Thermal Cycling Performance of EB-PVD TBCs Deposited under Different Processing Conditions

Dipak K. Das,[1,*] S. Gokul Lakshmi,[1] D. Srinivasa Rao,[2] S. Banumathy[1] and A. K. Singh[1]

[1] Defence Metallurgical Research Laboratory (DMRL), Kanchanbagh, Hyderabad 500058, India

[2] International Advanced Research Centre for Powder Metallurgy and New Materials (ARCI), Balapur P.O., Hyderabad 500005, India

Abstract. The microstructure, texture and thermal cycling life of a thermal barrier coating (TBC) deposited by electron beam physical vapour deposition method under several combinations of substrate pre-heat temperature and rotation speed, have been examined. The yttria stabilized zirconia ceramic coating of the TBC deposited on stationary samples predominantly showed ⟨111⟩ texture, although other texture components such as ⟨220⟩ and ⟨311⟩ were also present. The coatings on the rotated samples exhibited a predominant ⟨100⟩ texture. The ⟨111⟩ texture component was also present in these coatings in varying degrees. The intensity of ⟨111⟩ texture component in the coatings on the rotated samples decreased by increasing the substrate pre-heating temperature. The coating microstructures obtained under various processing conditions were consistent with the previously reported microstructures. No conclusive trend in the effect of texture present in the thermal barrier coatings on their thermal cycling life was observed in this study.

Keywords. Thermal barrier coatings, electron beam physical vapour deposition, crystallographic texture, X-ray diffraction, thermal cycling.

PACS®(2010). 81.40.Ef, 64.70.Hz, 81.15.-z, 61.05.C-.

1 Introduction

Thermal barrier coatings (TBCs) are applied on Ni-base superalloy components of gas turbine engines such as blades and nozzle guide vanes for enhancing their performance limits and/or durability [1]. TBCs are bi-layer coatings consisting of an inner metallic bond coat and an outer ceramic coating. While the bond coat provides high temperature oxidation resistance to the substrate superalloy, the ceramic layer imparts thermal insulation to the substrate [1]. At present, the most widely used TBCs on rotating airfoil components consist of a 7 mass% yttria-stabilized zirconia (7YSZ) ceramic coating and a platinum-aluminide (Pt-Al) bond coat. The 7YSZ layer is deposited by electron beam physical vapour deposition (EB-PVD) method to achieve the segmented columnar structure that provides excellent strain-tolerance and thermal shock resistance [1, 2]. It is well established that the columnar microstructure of EB-PVD TBCs induces a high in-plane compliance that is crucial to its strain tolerance and lifetime [3–5]. The thermal conductivity of the ceramic coating is also influenced by the pore architecture that develops during the deposition process [6, 7]. The above two dominant characteristics of the microstructure, namely the columnar morphology and the pore architecture, are related to the evolution of texture in the ceramic coating [8]. The preferred crystallographic orientation in the ceramic layer is a result of the unique pattern of vapour incidence (and shadowing) arising from the rotation of components over the EB-PVD source. The 7YSZ columns typically grow in ⟨100⟩ direction with pyramidal tips bound by four {111} planes. It has been suggested that such pyramidal morphology ensures stable propagation of the column tip by enabling all tip facets to capture equal amount of vapour flux [9].

Evolution of microstructural features of the YSZ layer and its crystallographic texture in terms of the various parameters associated with EB-PVD process has been studied by several investigators [8, 10–19]. The important among these parameters are vapour incidence angle (VIA) α, substrate rotation speed and substrate pre-heat temperature. In the present study, an evaluation of the effect of two important EB-PVD process parameters, namely the rotation speed and the temperature of the substrate, on the YSZ coating microstructure and texture has been carried out. One of the objectives of this study has been to examine the effect of processing conditions (and, hence, crystallographic texture) on the thermal cycling life of the deposited TBCs.

2 Experimental Details

Substrates used for TBC deposition were disc-shaped pieces of diameter 13 mm and height 3 mm, which were

* **Corresponding author:** Dipak K. Das, Dipak K. Das, Defence Metallurgical Research Laboratory (DMRL), Kanchanbgah, Hyderabad 500058, India; E-mail: dkdasabcd@gmail.com.

Received: February 2, 2011. Accepted: May 29, 2011.

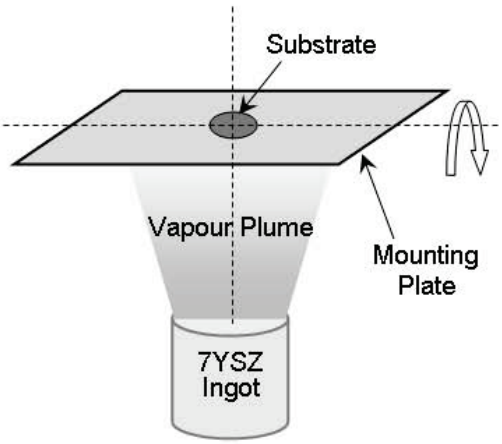

Figure 1. Schematic representation of the placement of the sample (substrate) with respect to the vapour plume during coating process.

Temperature (°C)	Rotation speed (rpm)	R_a of YSZ surface (μm)
1000	0 (Stationary)	1.47 ± 0.11
950	10	2.53 ± 0.12
950	20	2.72 ± 0.15
1000	10	2.16 ± 0.05
1000	20	2.19 ± 0.20
1050	10	1.84 ± 0.12
1050	20	2.39 ± 0.10

Table 1. Processing conditions for deposition of 7YSZ layer and the corresponding surface roughness (R_a) values.

sliced from directionally solidified (DS) rods of Ni-base superalloy CM-247LC using wire-cut method. The nominal composition (in mass%) of this alloy is 9.2 Co-8.1 Cr-9.5 W-5.6 Al-3.2 Ta-1.5 Hf-0.7 Ti-0.015 Zr-0.5 Mo-0.15 B-0.07 C-balance Ni. The sliced samples were then applied with a high activity Pt-Al bond coat. The details of the process for the application of the bond coat can be found elsewhere [20]. Since grit blasting of the sample surface was involved in application of the bond coat, the surface of the bond coated samples was somewhat rough with a roughness (R_a) value of 1.45 ± 0.13 μm. The bond coated samples were then isothermally oxidized at 1050°C for 10 h in air to develop a thermally grown oxide (TGO) layer of α-Al_2O_3 prior to deposition of YSZ coating. The thickness of the prior TGO layer was measured to be approximately 800 nm. One flat surface of each sample was then deposited with a layer of 7YSZ coating using a 250 kW EB-PVD facility equipped with four electron guns. The 7YSZ ingot used for the coating purpose was cylindrical in shape having a diameter 68.5 mm and a height of 50 mm. The substrates were mounted on a flat stainless steel plate rotating about a horizontal axis that is normal to the axis of the evaporating 7YSZ ingot (and that of the vapour plume), as schematically shown in Figure 1. The distance between the surface of the plate and that of the evaporating 7YSZ ingot was approximately 350 mm. The samples were so mounted on the holder that they would be directly on top of the evaporating ingot when facing downward. This produced a net VIA $= 0°$ for the coating surface of the samples. The coating chamber pressure was maintained at 0.013 Pa (10^{-4} Torr) during the deposition process. Prior to coating deposition, the substrate was pre-heated to a previously decided temperature by employing the same electron beams that were subsequently used for evaporation of the ingot. After the substrate reached the required pre-heat temperature, coating was deposited by either keeping the sample stationary (directly on top of the evaporating ingot with the coating surface facing downward) or by rotating it at a fixed rpm. Three substrate pre-heating temperatures, namely 950, 1000 and 1050°C, and three rotation speeds, viz. 0 (stationary), 10 and 20 rpm, were used for coating deposition. Coating deposition on the stationary sample was carried out for one substrate pre-heating temperature of 1000°C. Table 1 provides the various substrate temperature-rotation speed combinations under which the 7YSZ coating was deposited. The coating deposition was carried out for about 30 min on the stationary samples and for 45 min on the rotated samples.

X-ray diffraction (XRD) was used for examining the change in the preferred orientations of the deposited YSZ coatings. For comparison, the XRD pattern from the untextured (randomly oriented) 7YSZ powder was also obtained. The powder was produced by finely grinding a 7YSZ coating (deposited at 950°C, 20 rpm) after peeling it off from the substrate. The grinding of the coating was carried out by using an agate and mortar. The XRD patterns were recorded in a Philips 3020 diffractometer equipped with a graphite monochromater operated at 40 kV and 25 mA. The step size used in varying the diffraction angle (2θ) was 0.02° and the counting time at each step was 5 s. In order to compare the integrated intensity, all the samples were irradiated under identical conditions having equal irradiated area and same orientation. An Inel G3000 texture goniometer, coupled with curved position-sensitive detector and using Cu-K_α radiation, was also employed for texture investigation using Schultz reflection technique. The pole figures were corrected for defocusing and absorption using a powder sample.

The surface morphology and the cross-sectional microstructures of the coated samples were observed using a scanning electron microscope (SEM) operating at 20 kV. The roughness of the coated surface (R_a) for all the samples was measured using a Mitutoyo profile meter. Some

of the TBC coated samples were then subjected to thermal cycling at 1100°C in air. The test was carried out in an automated thermal cycling furnace. Each 1 h-cycle consisted of soaking the sample at 1100°C for 45 min followed by cooling in ambient air for 15 min outside the furnace.

3 Results and Discussion

3.1 X-ray Diffraction and Texture

Figure 2 presents the X-ray diffraction patterns for YSZ coatings deposited on the stationary sample and samples rotated at 10 rpm. For comparison, the pattern for the untextured YSZ powder has also been shown in the above figure. Tetragonal zirconia was detected in all the cases and the diffraction peaks in all the patterns, as shown in the above figure, corresponded to this phase. The same phase was also detected in case of coatings deposited at 20 rpm. The relative peak intensities of the various planes in the diffraction patterns are indicative of the textures present in the coatings. Based on the intensities from the coatings and those from the random (un-textured) 7YSZ powder, texture coefficients for all the coatings were calculated using the following formula (equation (1)) [21].

$$T_c(\text{hkl}) = \frac{I(\text{hkl})/I_R(\text{hkl})}{\frac{1}{n}\sum_i^n I(\text{hkl})/I_R(\text{hkl})}. \quad (1)$$

In the above equation T_c(hkl) represents the texture coefficient of (hkl) crystallographic planes in the coating, I(hkl) the corresponding integrated intensity, I_R(hkl) the integrated intensity from (hkl) planes in the un-textured specimen (i.e. 7YSZ powder), and n is the total number of reflections measured. The T_c values of the various planes

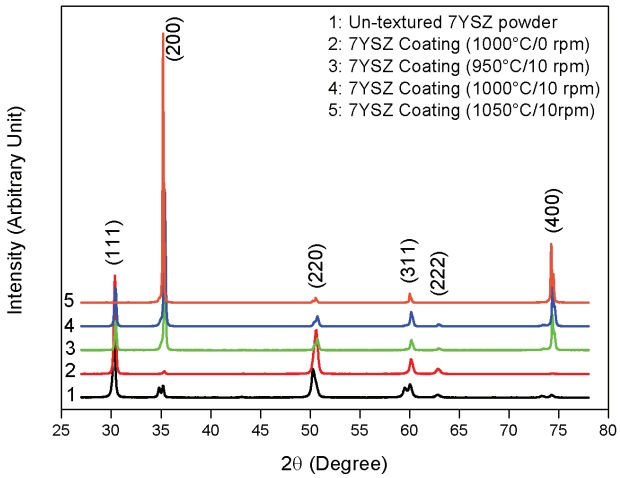

Figure 2. X-ray diffractograms for 7YSZ coating deposited using various deposition conditions. The XRD pattern corresponding to the untextured 7YSZ powder has also been included.

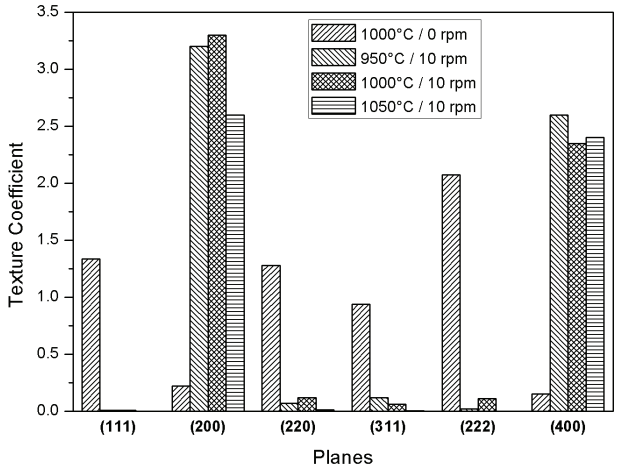

Figure 3. Texture coefficients of the various 7YSZ coatings deposited in this study.

in a coating essentially signify the extent of corresponding textures parallel to coating surface. The T_c values for the coatings deposited on the stationary sample and those rotated at 10 rpm are presented in the form of a bar chart in Figure 3. It is evident from the X-ray diffractograms in Figure 2 and the corresponding T_c values in Figure 3, that the growth direction of the columns in the coating was mostly along ⟨111⟩ in case of the stationary sample (0 rpm). However, a minor fraction of the columns also grew along ⟨220⟩ and ⟨311⟩ directions. In contrast, the coatings deposited on the rotated samples revealed a strong ⟨100⟩ orientation although the other orientations such as ⟨111⟩, ⟨220⟩ and ⟨311⟩ were also present. The ⟨100⟩ orientation of the coating is also evident from the presence of strong (200) and (400) peaks in the diffractograms (Figure 2). Several researchers have reported strong ⟨111⟩ and ⟨100⟩ orientations in case of stationary and rotated samples, respectively [12, 15–17]. They also have detected the additional reflections such as (220) and (311) in case of stationary substrate and (111), (220) and (311) in case of rotated substrate [15–17]. However, these additional reflections were detected only during early stages of coating deposition. For example, Wada et al. found that (200), (112), (220) and (311) reflections were detected in the coating on stationary sample up to about 12 s of deposition, beyond which only (111) reflections were detected. Similarly, in case of rotated substrates (5 and 10 rpm), the (111), (112), (220) and (311) reflections disappeared at various times between 36–300 s during coating deposition. Beyond 300 s, only (100) reflections were detected in the above coating [12, 15]. In the present case, however, the minor peaks did not disappear and were present along with the dominant peaks ((111) or (100)) in the final coating for all combinations of substrate temperature and rotation speeds (see Figure 2).

Figures 4(a) and (b) present the (111) and (200) pole figures for the YSZ layer which was deposited on the station-

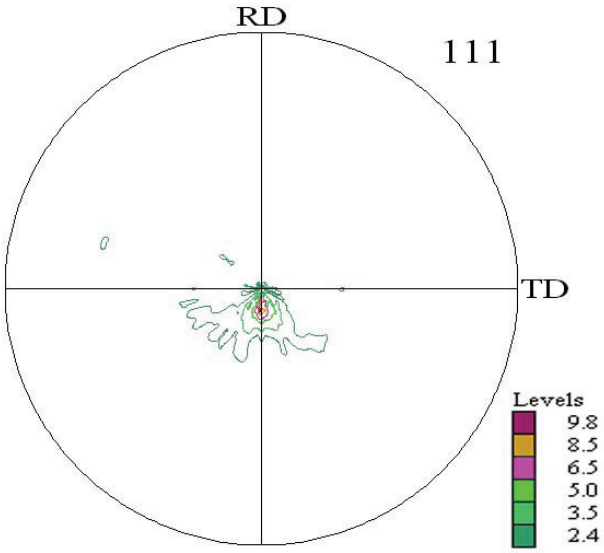

(a)

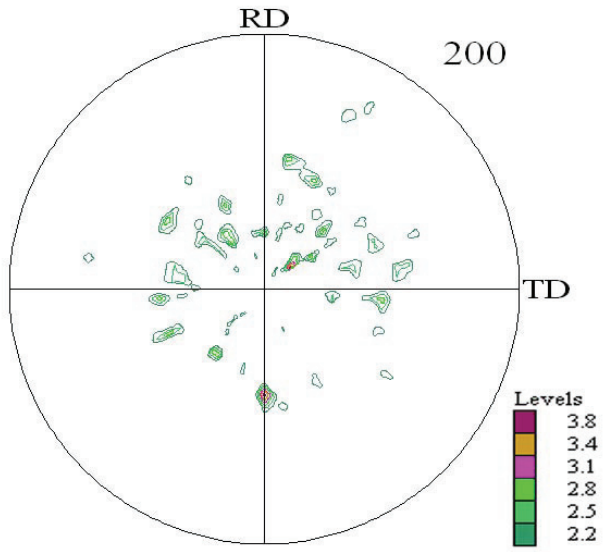

(b)

Figure 4. Pole figures for the 7YSZ coating deposited on a stationary (0 rpm/1000°C) sample: (a) (111) pole and (b) (200) pole.

ary sample. The (111) poles have marginally shifted (by about 10°) from the substrate normal (Figure 4(a)). The (200) pole displayed several isolated components with weak intensities around the centre of the pole figure, as shown in Figure 4(b). It is well known that the formation of ⟨111⟩ oriented columns is a characteristic of the coating layers deposited at low vapour incidence angles (VIA), typically less than 30° [14]. If the sample deposited at VIA = 0° is placed directly above the ingot source, as done in the present case of stationary substrate, in-plane orientation should not develop and the (200) pole would show a ring pattern around the centre, indicating a ⟨111⟩ fibre texture [14]. In the present case, the distributed intensities observed in (200) and strong ⟨111⟩ orientation in (111) pole figures (Figure 4) indicate that the YSZ layer deposited on the stationary sample did not develop perfect ⟨111⟩ fibre texture, possibly because of some degree of in-plane growth of the columns despite their strong out-of-plane growth. It is believed that the sample had not been positioned accurately on the mounting plate and, as a consequence, it did not remain directly above the vapour source during the deposition process. In other words, there was a slight shift in the position of the sample away from the centreline of the vapour plume, as shown in Figure 1. Such shift in position has been reported to cause the above mentioned in-plane orientation in the coating [13].

Figures 5(a) and (b) show the pole figures for the sample coated at 950°C/10 rpm. The four-fold symmetry of ⟨100⟩ texture in (111) pole figure, as reported in several studies [8, 14], can be clearly seen in Figure 5(a). The corresponding (200) pole figure, as shown in Figure 5(b), confirms the above observation. The ⟨100⟩ growth direction of the columns was not perfectly parallel to the substrate normal, as evident from the marginal (about 5°) shift of the peak intensity from the centre of the (200) pole figure (Figure 5(b)). Apart from the dominant ⟨100⟩ texture, the presence of a weak ⟨111⟩ texture component could also be observed in the (111) pole figure (Figure 5(a)). By increasing the rotation speed to 20 rpm at the same substrate temperature of 950°C, the overall nature of texture in terms of (111) and (200) pole figures did not change appreciably, except slight variations in the intensities of the texture components (Figure 5(c) and (d)). However, using a substrate temperature of 1000°C led to a considerable reduction in the intensity of the ⟨111⟩ texture component at both rotation speeds (10 and 20 rpm). Increasing the substrate temperature further to 1050°C, the ⟨111⟩ component was eliminated and the growth direction of the YSZ columns of the coating was solely ⟨100⟩ at both the rotation speeds, as evident from Figure 6(a)–(d). From the above observations, it is apparent that the pre-heat temperature of the substrate has a significant effect on the texture that develops in the 7YSZ coating. However, the rotation speed (10 or 20 rpm) does not appear to appreciably influence the coating texture at any given substrate temperature.

Wada et al. [11] have reported the effect of substrate preheating temperature on crystallographic texture that develops during the deposition of a 4 mass% YSZ coating on rotating (5 rpm) substrates. They observed that the growth direction of the columns in the coating was predominantly ⟨111⟩ up to a substrate temperature of about 750°C. Above 938°C, the dominant orientation in the coating was ⟨100⟩. In the present case of rotated samples also, the dominant crystal orientation was ⟨100⟩, although a weak ⟨111⟩ component persisted in case of substrate pre-heat temperature of 950°C (Figures 5 and 6). Only above 1000°C, the ⟨111⟩

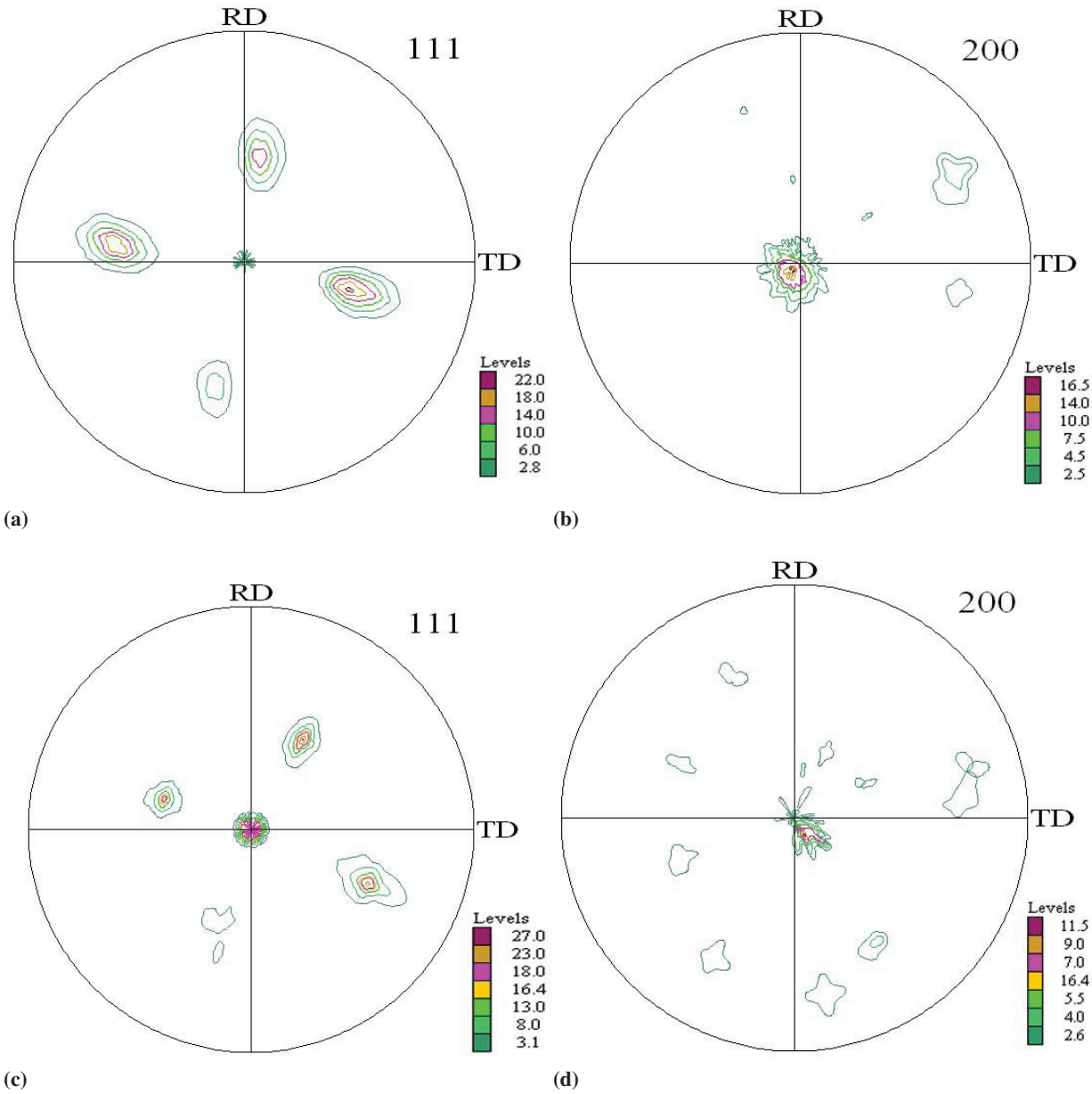

Figure 5. Pole figures for the 7YSZ coating deposited on a rotated sample with substrate pre-heating temperature of 950°C: (a–b) 10 rpm and (c–d) 20 rpm.

component became negligibly weak and ⟨100⟩ texture completely dominated the coating. The above mentioned observations made from texture analysis of the coatings are consistent with the texture coefficient results mentioned previously (Figure 3).

3.2 Surface Morphology and Microstructure of Coatings

The surface morphology of the coating on the stationary sample revealed columns with triangular facets (Figure 7(a)) which is consistent with the predominant ⟨111⟩ crystal orientation present in this coating [14, 16]. The dense coating microstructure observed in this case (Figure 7(b)) is also consistent with similar structures reported in other studies [14]. In case of rotated substrates, well-defined pyramidal-tipped columns developed at all three substrate temperatures [14, 17]. A typical case is shown in Figure 8(a) where the deposition was carried out at 1000°C/20 rpm. No appreciable effect of rotation speed on the surface morphology was observed for all three substrate temperatures. The surface roughness (R_a) values for all the 7YSZ layers are provided in Table 1. It is evident

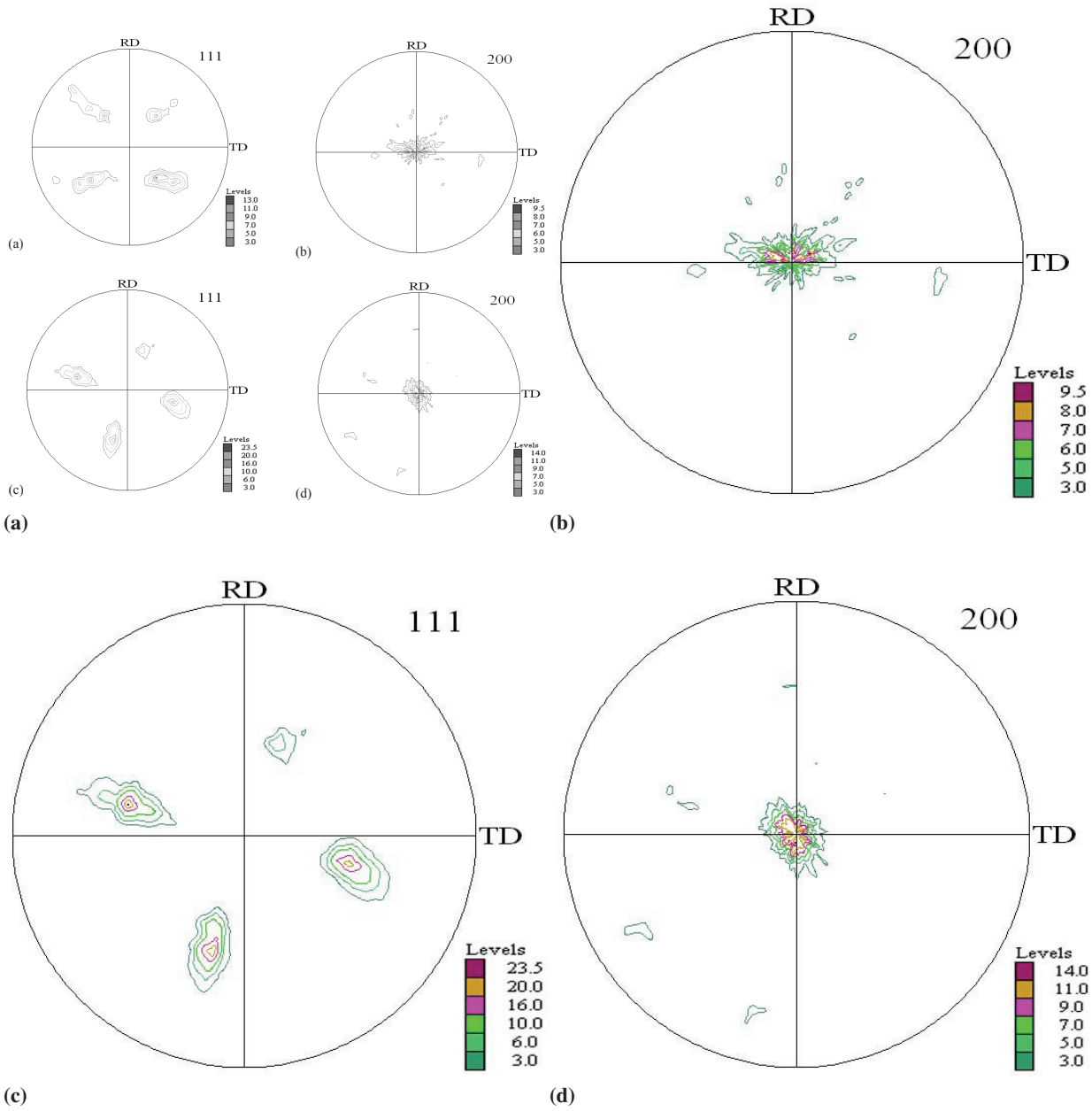

Figure 6. Pole figures for the 7YSZ coating deposited on a rotated sample with substrate pre-heating temperature of 1050°C: (a–b) 10 rpm and (c–d) 20 rpm.

that the R_a values, which lied in the approximate range of 1.5–2.7 μm, are close to the value of 1.5 μm reported by Das et al. for another EB-PVD thermal barrier coating [22]. The minimum surface roughness (1.47 μm) in case of the coating on stationary sample is to be expected considering the fact the coating was dense and consisted of much finer columns as compared to the coatings on rotated samples [14].

Table 2 presents the thickness of the coatings achieved under various processing conditions. As evident, the coating thickness varied in the range of 80-170 μm. It is also evident that the deposition rate, and hence the coating thickness, was 25-50% higher at 20 rpm than at 10 rpm at all three substrate pre-heat temperatures. Further, the deposition rate for the stationary sample was appreciably higher than the rates for to the corresponding rotating samples. A similar dependence of the rotation speed with the deposition rate has also been reported by Zhao et al. [16]. They found the deposition rate (at 1000°C) for the stationary sample to be nearly 4–5 times of the values obtained with 12–20 rpm.

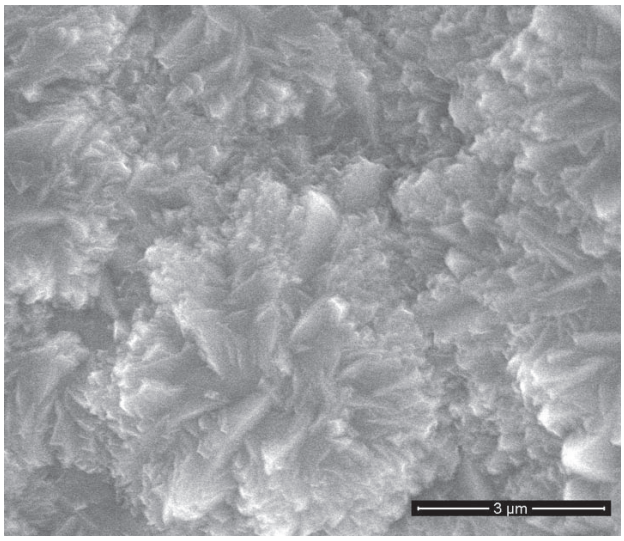

(a)

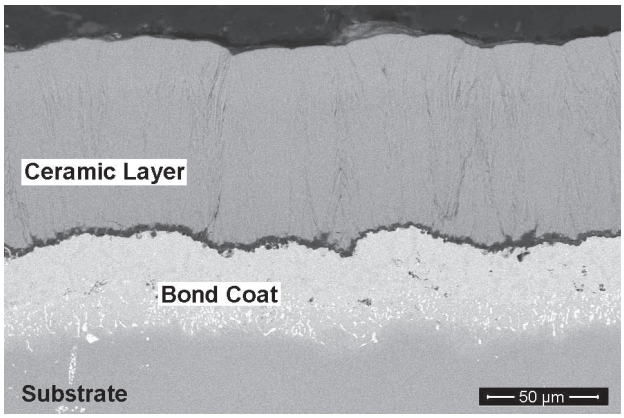

(b)

Figure 7. The 7YSZ coating deposited on a stationary (0 rpm/1000°C) sample: (a) surface morphology and (b) cross-sectional microstructure.

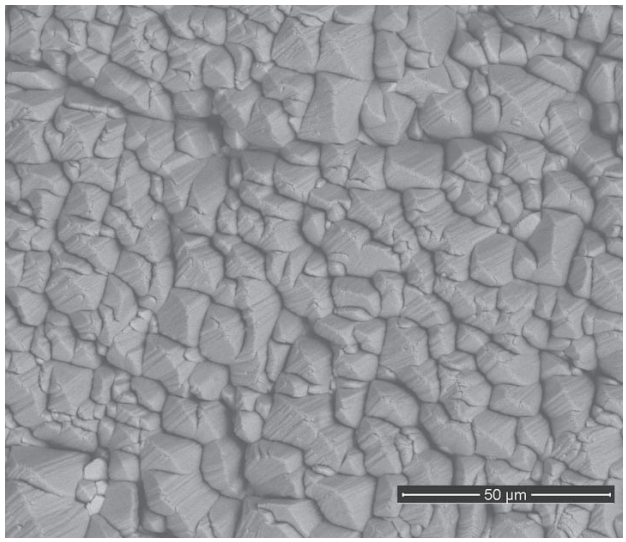

(a)

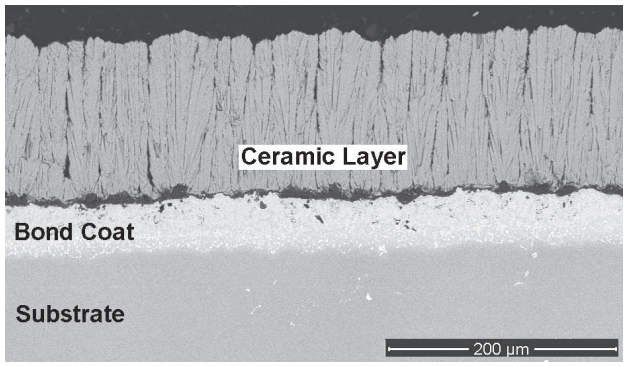

(b)

Figure 8. The typical 7YSZ coating deposited on a rotated sample (1000°C/20 rpm): (a) surface morphology and (b) cross-sectional microstructure.

Substrate Temperature (°C)	Rotation speed (rpm)	Deposition duration (min)	YSZ layer (µm)	Deposition rate (µm min^{-1})
950	10	45	110	2.44
	20	45	170	3.77
1000	0 (Stationary)	30	85	2.83
	10	45	88	1.96
	20	45	110	2.44
1050	10	45	80	1.78
	20	45	115	2.56

Table 2. Thickness and deposition rate of the YSZ coatings obtained under various processing conditions.

They also observed the coating deposition rate at 12 rpm to be somewhat higher than that at 20 rpm. Figure 8(b) show the typical cross-sectional micrograph of the YSZ coating on rotated samples. In all these cases, columns were nearly perpendicular to the surface of the bond coated substrate. As expected, the column width was minimum at the bond coat/YSZ interface and maximum at the surface of the YSZ coating.

The differences in microstructure, surface morphology and deposition rate of the coating between the stationary and rotated substrates can be explained in terms of the associated deposition mechanisms, as suggested by Jang and Matsubara [15]. When the substrate is stationary (0 rpm), it is always exposed to a uniform vapour flux. Therefore, the deposition rate is fast and the vapour flow is constant. As a result, the columns grow uniformly and do not develop any appreciable porosity, leading to a dense structure (Figure 7(b)) [16]. In contrast, for rotated specimens, the

deposition rate is slower and the microscopic vapour flow is non-uniform because of the disturbance caused by the substrate rotation in a sunrise/sunset manner. Such slow deposition rates induce competitive growth of the columns and cause shadow areas, where competitively growing crystals screen or shield adjacent regions from growing. Such shadow areas remain in the coating as inter-column and other types of porosities [15, 23, 24], as was observed in present case of the rotated samples (Figure 8(b)). It has been shown that the shadow areas, i.e. the coating porosity, increase with the increase in rotation speed. At low speeds (0–5 rpm), the columns constituting the coating develop a wavy or zigzag morphology [12, 14–16]. At higher rotation speeds (5–20 rpm), however, such morphology is not observed and the coating develops straight pyramidal columns [12, 15]. In the present case, the absence of any significant effect of the rotation speeds on the coating structure can be ascribed to the higher rpm values (10 and 20) used for coating deposition.

The YSZ coating microstructures obtained in the EB-PVD process have been explained on the basis of the 'structure zone model' which was proposed by Movchan and Demchishin [25, 26]. According to this model, the microstructure of the coating layer can be categorized into three zones in terms of the homologous temperature T_H, where $T_H = T_s/T_m$. T_s and T_m (in Kelvin) correspond to substrate temperature and the melting temperature of the coating material (7YSZ in the present case), respectively. Zone 1 ($T_H < 0.3$) consists of dome-topped and tapered crystals separated by voided boundaries. In this zone, insufficient surface diffusion of adatoms and the shadowing effect dominate the formation of the coating structure. In Zone 2 ($T_H = 0.3$–0.5), the coating develops smooth or faceted surfaces and dense columnar grains caused by surface diffusion dominant condensation. Coatings formed in Zone 3 ($T_H > 0.5$) develop equiaxed grains resulting from bulk diffusion mechanisms. Well-developed pyramidal columns form in the coating when T_H lies in the approximate range of 0.26–0.45. In the present study, T_H values corresponding to substrate temperatures of 950, 1000 and 1050°C were 0.41, 0.43 and 0.44, respectively. The pyramidal-column structure of the coatings on the rotated samples (Figure 8(b)) is, therefore, consistent with the model suggested by Movchan and Demchishin [25].

3.3 Thermal Cycling Performance

As mentioned previously, the coated samples were subjected to thermal cycling in air at 1100°C. The 7YSZ layer spalled after certain number of cycles under the action of cyclic heating and cooling. Thermal cycling life for a coating has been defined as the number of cycles after which 50% or more portion of the ceramic layer spalled from the coated surface of the sample [27]. Figure 9 presents the cycling lives of the coatings deposited with various combinations of substrate temperature and rotation speeds. The life varied between a minimum of 100 cycles to a maximum of 275 cycles. These values were considerably lower than about 700–1000 cycles reported for TBCs in other studies [28–30]. It may be noted that the thermal cycling performance of the coatings deposited at 20 rpm (at all three temperatures) was relatively better (> 200 cycles) than that of the coatings deposited at 10 rpm (Figure 9). This is consistent with the results of Matsumoto et al. who have observed an increase in cycling life (evaluated at 1150°C) with increase in the rotation speed in case of 4YSZ coating on Inconel 738LC superalloy [31]. As mentioned previously (Table 2), the coatings deposited at 20 rpm had much higher thickness as compared to those deposited at 10 rpm. The higher thickness of the latter coatings would cause higher residual stresses during thermal cycling, resulting in their faster failure, as observed in the present study (Figure 9). Matsumoto et al. [31] found that the cycling life in case of the stationary samples was the minimum. This was, however, not the case in the present study. In fact, the TBC on stationary samples exhibited a life of 225 cycles (Figure 9), which was comparable with that of the samples coated at 20 rpm. Thus, no conclusive trend on the dependence of thermal cycling life on the coating deposition conditions (and, hence, the coating texture) was apparent from this study. Coatings with both ⟨111⟩ texture (stationary sample) and ⟨100⟩ texture (rotated samples) showed comparable lives in the range of 100–275 cycles. Therefore, a more detailed study is necessary to determine the effect, if any, of crystallographic texture in TBCs on their thermal cycling life.

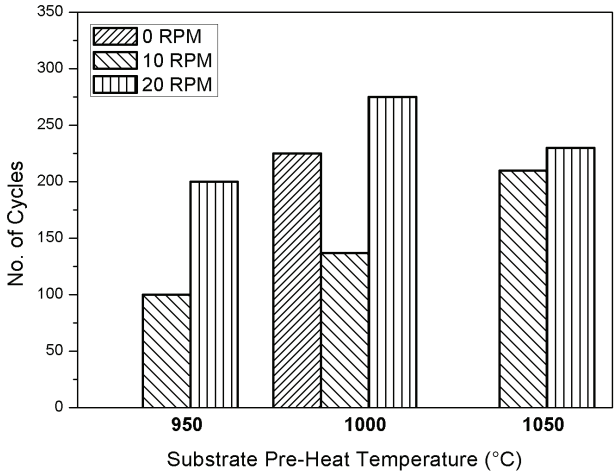

Figure 9. Thermal cycling lives of the various 7YSZ coatings tested at 1100°C in air.

4 Conclusions

In the present study, microstructure, texture and thermal cycling life of a set of TBCs deposited on CM-247LC super-

alloy samples by EB-PVD technique, have been examined. The 7YSZ ceramic layer of the TBCs was deposited using various combinations of substrate pre-heat temperature and rotation speed. Although ⟨111⟩ texture was predominant in the 7YSZ coating deposited on stationary (non-rotated) samples, other texture components such as ⟨220⟩ and ⟨311⟩ were also present in the coating. The coatings on rotated samples (rotation speeds of 10 and 20 rpm) exhibited predominant ⟨100⟩ texture, although the ⟨111⟩ component was also observed in varying degrees. In these coatings, the ⟨111⟩ texture component decreased by increasing the substrate pre-heat temperature. The coating on the stationary sample showed a dense structure consisting of extremely fine columns. However, a much coarser coating structure comprising of pyramidal columns was observed in case of the rotated samples. The coating microstructures have been explained in terms the associated coating deposition mechanisms. In this study, no conclusive trend in the effect of texture present in the TBCs on their thermal cycling life was observed.

Acknowledgments

The authors would like to thank the Metallography and Electron Microscopy groups of DMRL for their support. They are extremely thankful to Mr. C. Mondal for extensive technical discussions. They also wish to thank Director, DMRL for his permission to publish this work. The financial support for this research activity has been provided by DRDO.

References

[1] D. R. Clarke and C. G. Levi, Materials design for the next generation thermal barrier coatings, Annu. Rev. Mater. Res., 33 (2003), 383–417.

[2] J. T. DeMasi-Marcin and D. K. Gupta, Protective coatings in the gas turbine engine, Surf. Coat. Technol., 68–69 (1994), 1–9.

[3] T. E. Strangman, Thermal barrier coatings for turbine airfoils, Thin Solid Films, 127 (1985), 93–106.

[4] C. A. Johnson, J. A. Ruud, R. Bruce and D. J. Wortman, Relationships between residual stress, microstructure and mechanical properties of electron beam –physical vapour deposition thermal barrier coatings, Surf. Coat. Technol., 108/109 (1998), 80–85.

[5] U. Schulz, K. Fritscher, C. Leyens and M. Peters, Influence of processing on microstructure and performance of electron beam physical vapour deposition (EB-PVD) thermal barrier coatings, J. Engineering for Gas Turbines and Power, 124 (2002), 229–34.

[6] S. Gu, T. J. Lu, D. D. Hass and H. N. G. Wadley, Thermal conductivity of zirconia coatings with zig-zag pore microstructures, Acta mater., 49 (2001), 2539–2547.

[7] T. J. Lu, C. G. Levi, H. N. G. Wadley and A. G. Evans, Porosity as a control parameter for oxide thermal barriers made by physical vapour deposition, J. Am. Ceram. Soc., 84 (2001), 2937–2946.

[8] U. Schultz, H. Oettel and W. Bunk, Texture of EB-PVD thermal barrier coatings deposited under variable deposition conditions, Z. Metallkd., 87 (1996), 488–492.

[9] Scott G. Terry, Jennifer R. Litty and Carlos G. Levi, Evolution of porosity and texture in thermal barrier coatings grown by EB-PVD, in Elevated Temperature Coatings: Science and Technology III, J. M. Hampikian and N. B. Dahotre (eds.), The Minerals, Metals and Materials Society, Warrendale, PA, 1999, pp. 13–26.

[10] J. S. Bernier, G. Levan, Md. Maniruzzaman, R. D. Sisson Jr. and S. Bose, Crystallographic texture of EB-PVD TBCs deposited on stationary flat surfaces in a multiple ingot coating chamber as a function of chamber position, Surf. Coat. Technol., 163–164 (2003) 95–99.

[11] K. Wada, N. Yamaguchi and H. Matsubara, Crystallographic texture evolution in ZrO_2-Y_2O_3 layers produced by electron beam physical vapour deposition, Surf. Coat. Technol., 184 (2004), 55–62.

[12] B. K. Jang and H. Matsubara, Influence of rotation speed on microstructure and thermal conductivity of nano-porous zirconia layers fabricated by EB-PVD, Scripta mater., 52 (2005), 553–558.

[13] K. Wada, M. Yoshiya, N. Yamaguchi and H. Matsubara, Texture and microstructure of ZrO_2-4 mol% Y_2O_3 layers obliquely deposited by EB-PVD, Surf. Coat. Technol., 200 (2005), 2725–2730.

[14] K. Wada, N. Yamaguchi and H. Matsubara, Effect of substrate rotation on texture evolution in ZrO_2-4mol.%Y_2O_3 layers fabricated by EB-PVD, Surf. Coat. Technol., 191 (2005), 367–374.

[15] B. K. Jang and H. Matsubara, Surface roughness and microstructure of yttria stabilized zirconia EB-PVD coatings, Surf. Coat. Technol., 200 (2006), 4594–4600.

[16] H. Zhao, F. Yu, T. D. Bennett and H. N. G. Wadley, Morphology and thermal conductivity of yttria-stabilized zirconia coatings, Acta mater., 54 (2006), 5195–5207.

[17] U. Schulz, S. G. Terry and C. G. Levi, Microstructure and texture of EB-PVD TBCs grown under different rotation modes, Mater. Sci. Eng. A, A360 (2003), 319–329.

[18] N. Zotov, M. Bartsch, L. Chernova, D. A. Schmidt, M. Havenith and G. Eggeler, Effects of annealing on the microstructure and the mechanical properties of EB-PVD thermal barrier coatings, Surf. Coat. Technol., 205 (2010), 452–464.

[19] D. S. Rao, K. Valleti and S. V. Joshi, Processing-structure-property relationships in electron beam physical vapour deposited yttria stabilized zirconia coatings, J. Vac. Sci. Technol. A, 29 (2011), DOI:10.1116/1.3563600.

[20] D. K. Das, V. Singh and S. V. Joshi, Effect of pre-aluminizing diffusion treatment on microstructural evolution of high activity Pt-aluminide coatings, Metall. Mater. Trans. A, 31A (2000), 2037–2047.

[21] B. D. Cullity, Elements of X-ray Diffraction, Addison-Wesley Publishing Company, Reading, MA (1978).

[22] D. K. Das J. P. McDonald, S. M. Yalisove and T. M. Pollock, Femtosecond pulsed laser damage characteristics of 7% Y_2O_3-ZrO_2 thermal barrier coating, Appl. Phys. A, 91 (2008), 421–428.

[23] U. Schulz, Thermal cyclic behaviour of microstructurally modified EB-PVD thermal barrier coatings, Mater. Sci. Forum, 251 -254 (1997), 957–964.

[24] U. Schulz, K. Fritscher and M. Peters, EB-PVD Y_2O_3- and CeO_2/Y_2O_3- stabilized zirconia thermal barrier coating –

crystal habit and phase composition, Surf. Coat. Technol., 82 (1996), 259–269.

[25] B. A. Movchan and A. V. Demchishin, Study of the structure and properties of thick vacuum condensates of nickel, titanium, tungsten, aluminium oxide and zirconium oxide, Phys. Met. Metallogr., 28 (1969), 83–90.

[26] J. A. Thornton, High rate thick film growth, Ann. Rev. Mater. Sci., 7 (1977), 239–260.

[27] S. Sridharan, L. Xie, E. H. Jordan and M. Gell, Stress variation with thermal cycling in the thermally grown oxide of EBPVD thermal barrier coating, Surf. Coat. Technol., 179 (2004), 286–296.

[28] S. Sridharan, L. Xie, E. H. Jordan, M. Gell and K. S. Murphy, Damage evolution in an electron beam physical vapor deposited thermal barrier coating as a function of cycle temperature and time, Mater. Sci. Eng. A, 393 (2005), 51–62.

[29] M. Wen, E. H. Jordan and M. Gell, Effect of temperature on rumpling and thermally grown oxide stress in an EB-PVD thermal barrier coating, Surf. Coat. Technol., 201 (2006), 3289–3298.

[30] D. K. Das and T. M. Pollock, Femtosecond laser machining of cooling holes in thermal barrier coated CMSX4 superalloy, J. Mater. Proc. Technol., 209 (2009), 5661–5668.

[31] M. Matsumoto, K. Wada, N. Yamaguchi, T. Kato and H. Matsubara, Effects of substrate rotation speed during deposition on the thermal cycle life of thermal barrier coatings fabricated by electron beam physical vapour deposition, Surf. Coat. Technol., 202 (2008), 3507–3512.